ACS Biomaterials SCIENCE & ENGINEERING

Article

pubs.acs.org/journal/abseba

Nanoengineered Osteoinductive and Elastomeric Scaffolds for Bone Tissue Engineering

Punyavee Kerativitayanan,[†] Marco Tatullo,[‡,§] Margarita Khariton,[†] Pooja Joshi,[†] Barbara Perniconi,[‡] and Akhilesh K. Gaharwar*[,†,∥,⊥]

[†]Department of Biomedical Engineering and [∥]Department of Materials Science and Engineering, Texas A&M University, College Station, Texas 77841, United States

[‡]Maxillofacial Unit, Calabrodental Clinic, 88900 Crotone, Italy

[§]Regenerative Medicine Section, Tecnologica Research Institute, 88900 Crotone, Italy

[⊥]Center for Remote Health Technologies and Systems, Texas A&M University, College Station, Texas 77843, United States

ABSTRACT: Synthesis and fabrication of porous and elastomeric nanocomposite scaffolds from biodegradable poly(glycerol sebacate) (PGS) and osteoinductive nanosilicates is reported. Nanosilicates are mineral-based two-dimensional (2D) nanomaterials with high surface area which reinforced PGS network. The addition of nanosilicates to PGS resulted in mechanically stiff and elastomeric nanocomposites. The degradation rate and mechanical stiffness of nanocomposite network could be modulated by addition of nanosilicates. Nanocomposite scaffolds supported cell adhesion, spreading, and proliferation and promoted osteogenic differentiation of preosteoblasts. The addition of nanosilicates to PGS scaffolds increased alkaline phosphatase (ALP) activity and production of matrix mineralization. In vivo studies demonstrated biocompatibility and biodegradability of nanocomposite scaffolds. Overall, the combination of elasticity and tailorable stiffness, tunable degradation profiles, and the osteoinductive capability of the scaffolds offer a promising approach for bone tissue engineering.

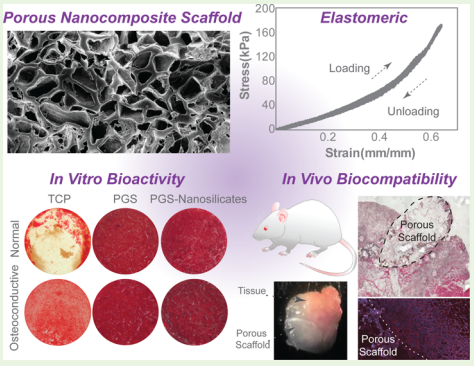

KEYWORDS: *nanocomposites, poly(glycerol sebacate) (PGS), two-dimensional (2D) nanosilicates, biocompatibility, osteoinductive*

INTRODUCTION

More than 2.2 million bone grafting surgeries are performed worldwide each year, costing approximately 2.5 billion US dollars annually; that number is expected to rise because of the aging population.[1,2] Although autografting is the clinical gold standard as it provides optimal osteogenesis, it results in donor site morbidity and postoperation complications including hernia formation, nerve injury, blood loss, and infection.[3−5] Allografting is the surgeon's second choice, but can result in immunogenic reactions and risk of disease transmission.[6−10] Allograft processing, including freezing and irradiation, can mitigate these risks, but at the same time weaken its biomechanical and biochemical characteristics. Demineralized bone matrix (DBM) is another available option, but it suffers from nonuniform processing procedures.[6−10] Consequently, DBM is mostly used as a bone graft extender rather than a sole bone graft substitute. Because of above limitations, there is an unmet need to develop synthetic bone graft substitutes to promote bone regeneration.

Macroporous bioactive ceramic granules are the most popular among synthetic bone grafts and bone graft substitutes. Surgeons mix these ceramic granules with patients' blood and use as a putty to fill bone defects.[6−10] Synthetic hydroxyapatite (sHAp), beta tricalcium phosphate (β-TCP), and biphasic calcium phosphate (a mixture of sHAp and β-TCP) are most commonly used as ceramic granules.[9] Compared to sHAp, bioactive glasses (Na_2O-CaO-P_2O_5-SiO_2) exhibit 10-fold higher bioactivity index, indicating superior bone bonding ability. Nevertheless, translational success of these osteoconductive biomaterials has been restricted due to limited mechanical stability.[10−12] Therefore, there is a demand for alternative materials such as nanocomposites to control and direct cell function for bone regeneration.[13−16]

In this regard, we recently reported that two-dimensional (2D) nanosilicates (Laponite, $Na^+_{0.7}[(Mg_{5.5}Li_{0.3})Si_8O_{20}(OH)_4]^-_{0.7}$) induce osteogenic differentiation of human mesenchymal stem cells (hMSCs) without any osteoinductive supplements such as bone morphogenic protein-2 (BMP-2).[16−19] Osteoinductive properties of nanosilicates stem from their dissolution products, i.e., Na^+, Mg^{2+}, Li^+, and $Si(OH)_4$. Specifically, magnesium ions (Mg^{2+}) were reported to promote adhesion of osteoblasts to material surfaces via fibronectin receptor $\alpha_5\beta_1$ and β_1 integrins, which brought about ossification and increased extracellular matrix protein expression.[20,21] Lithium ions (Li^+) activated the Wnt/β-catenin signaling pathway. This pathway activation resulted in increased cell proliferation and matrix mineralization. It also promoted osteogenic differentiation of mesenchymal cells

Received: January 13, 2017
Accepted: March 3, 2017
Published: March 3, 2017

DOI: 10.1021/acsbiomaterials.7b00029
ACS Biomater. Sci. Eng. 2017, 3, 590−600

while inhibiting osteoclastogenesis and apoptosis.[22] Orthosilicic acid ($Si(OH)_4$) stimulated osteogenic differentiation as well as promoted collagen type I synthesis.[20,23] Moreover, cytotoxic concentration of nanosilicates was 10-fold higher than that of sHAp, suggesting that significantly higher dose of nanosilicates could be tolerated by cells.[17] Possessing these properties, nanosilicates offer a growth factor-free approach for bone regeneration, minimizing complexities and expenses involved in growth factor delivery.

Because nanosilicates have heterogeneous charge distribution, they interact strongly with hydrophilic polymers such as collagen and poly(ethylene glycol) (PEG)[13,14] and have be developed as high performance elastomers,[24−27] moldable hydrogels,[28] injectable hemostats,[29] self-healing structures,[30] and drug delivery vehicles.[31−33] Our group recently reported that incorporation of nanosilicates in collagen-based hydrogels gave rise to a 4-fold increase in bone formation without any osteoinductive factors.[19,34] However, development of osteoinductive scaffolds with load-transducing mechanical properties remains a significant challenge. It is important to note that bone is a dynamic tissue where remodeling continuously takes place. Applied loads play critical roles in determining the rate of turnover as well as the formation of callus, its volume, and stiffness during bone healing. Thus, scaffolds with tailorable mechanical properties and degradation kinetics are of pivotal importance.

Here, we report the fabrication of porous poly(glycerol sebacate) (PGS)/nanosilicates nanocomposites scaffolds for bone tissue engineering. PGS is elastomeric and tough polyester, and undergoes surface erosion, making it appropriate for tissue engineering scaffolds.[35−37] The degradation products are completely resorbable and have shown to trigger minimum inflammation and limited fibrous encapsulation compared to other synthetic polymers such as poly(lactic-*co*-glycolic acid) (PLGA) and poly(lactic acid) (PLA).[35−37] PGS is also osteoconductive and supports adhesion and differentiation of preosteoblasts in vitro.[38] Because PGS has been shown to be osteoconductive, its action is expected to complement the osteoinductive capability of nanosilicates, resulting in enhanced bone regeneration. Furthermore, PGS could induce angiogenesis, contributing to its extensive studies as a vascular graft.[38,39] Because angiogenesis is generally coupled with osteogenesis, this property stresses its potential for bone tissue engineering.

■ MATERIALS AND METHODS

Poly(glycerol sebacate) (PGS) Synthesis. Polycondensation of glycerol (Sigma-Aldrich) and sebacic acid (Sigma-Aldrich) in a 1:1 molar ratio was performed following published procedures to obtain PGS prepolymer.[40,41] Briefly, equimolar ratios of glycerol and sebacic acid were allowed to react under nitrogen in a three-neck flask (round-bottom) at 120 °C. The vacuum (50 mTorr) was turned on after 60 min and the reaction was allowed to continue for 2 days. After the reaction was finished, the vacuum was turned off and polymer was cooled down to room temperature (under argon) and kept at 4 °C for storage.

Fabrication of PGS and PGS/Nanosilicates (PGS/nSi) Scaffolds. Porous scaffolds were fabricated by salt-leaching method. Briefly, NaCl (Sigma-Aldrich, ACS reagent grade) was grinded using a mortar and pestle, and then sieved to gather crystals that fall between 75 and 150 μm diameter to use as porogens. VWR sieves #100 (150 μm opening) and #200 (75 μm opening) were used. Teflon molds were completely filled with sieved salts, and put into an oven overnight at 37 °C. The Teflon molds were custom-made to have a size of 6 mm diameter and 2 mm thickness. Next, in a glass vial, PGS was dissolved in 30%ethanol/70%chloroform (50% w/v), then 0, 1, 2.5, 5, and 10% of nanosilicates was added. Nanosilicates (Laponite XLG) was obtained from BYK Additives Inc. Nanosilicates are 2D nanoclays with 20−50 nm in diameter and 1 nm in thickness with chemical formula $-(Na^{+}_{0.7}[(Mg_{5.5}Li_{0.3})Si_8O_{20}(OH)_4]^{-}_{0.7})$. A probe sonicator (FB120, Fisher Scientific) was used to mix nanosilicates in PGS solution until it turned homogeneous. The solution was added to the molds over the salt and allowed to penetrate between salt crystals until all the spaces were filled. The samples were kept in a fume hood for 48 h or until the solvent completely evaporated, then another 24 h in a vacuum desiccator for air bubble elimination. After that, the samples were thermally cured under vacuum at 130 °C for 48 h to covalently cross-link PGS prepolymer, similar to our previously published results.[40,41] Then, the cross-linked samples were removed from the molds and submerged in deionized water under agitation to leach out the salt. The salt leaching process took 36 h, with water changed every 4 h for the first 12 h. The scaffolds were lyophilized and stored in a vacuum desiccator until further studies.

Surface and Cross-Section Morphology. After successful fabrication, surface and cross-section images of the scaffolds were taken using a scanning electron microscope (SEM) (Neoscope JCM-5000). For cross-section imaging, the scaffolds were broken in half while submerged in liquid nitrogen in order to preserve their porous structure. The samples were kept in a vacuum desiccator for at least 24 h for drying before being mounted on specimen stubs using a carbon tape. They were then sputter-coated with gold/palladium before SEM imaging.

Mechanical Properties. Mechanical properties were studied using cyclic compression testing (eXpert 7600, ADMET, USA) with the strain rate of 1 mm/min until 60% strain for 8 cycles. From the stress−strain curves, compressive modulus, energy dissipation, and percent recovery upon reloading were calculated.

Degradation Studies. Scaffolds were first weighed for initial dry weight (W_i). They were then submersed in 0.01 M NaOH over a 1 week period at 37 °C. After 1, 2, 4, 7 days, the samples were collected and lyophilized, and final dry weight (W_d) was measured. Eq 1 was used to calculate the loss in weight in percent given the initial weight (W_i) and final dry weight (W_d).

$$\text{Weight loss (\%)} = \frac{W_i - W_d}{W_i} 100 \quad (1)$$

Protein Adsorption. Fetal bovine serum (FBS) protein was used for protein adsorption study. Scaffolds were washed thoroughly with Dulbecco's phosphate buffered saline (DPBS) before being incubated in 10% FBS at 37 °C, 5% CO_2, for 24 h. Note that FBS purchased from Life Technologies was diluted with DPBS to make 10% FBS solution. After 24 h, FBS was removed and the scaffolds were washed thrice with DPBS. The purpose of this washing step is to remove the proteins not being adsorbed on the scaffolds, so it should be gently done. After that, 2% sodium dodecyl sulfate (SDS) solution was added, and the well plate was shaken for 6 h to detach adsorbed proteins. The solution was then collected for protein assay. Note that SDS solution (20%) purchased from Amresco was diluted by DPBS to make 2% SDS solution used in the study. Protein concentration was determined using a Micro BCA Protein Assay Kit (Thermo Scientific) following manufacturer's protocols.

Cell Culture and in Vitro Cell Adhesion. MC-3T3 E1-subclone4 preosteoblasts (ATCC) were cultured in alpha modification of Eagle's medium (α-MEM, Hyclone) supplemented with 10% FBS and 1% Pen/Strep antibiotic (Life Technologies), in a humidified incubator at 37 °C and 5% CO_2 level. This medium would be referred to as normal growth media in this paper. The cells were harvested at 70% confluency for experiments. For sterilization, scaffolds were washed twice with DPBS then exposed to ultraviolet irradiation for 4 h. The scaffolds were soaked in normal growth media in an incubator overnight prior to cell seeding to pretreat the surface which would subsequently facilitate cell attachment. It should be noted that for all cell studies, cell-seeded scaffolds were cultured in nontreated well plates to minimize cell adhesion to the well plate (i.e., maximize cell adhesion to the samples), whereas cells seeded on treated well plates (referred to as tissue culture

DOI: 10.1021/acsbiomaterials.7b00029
ACS Biomater. Sci. Eng. 2017, 3, 590−600

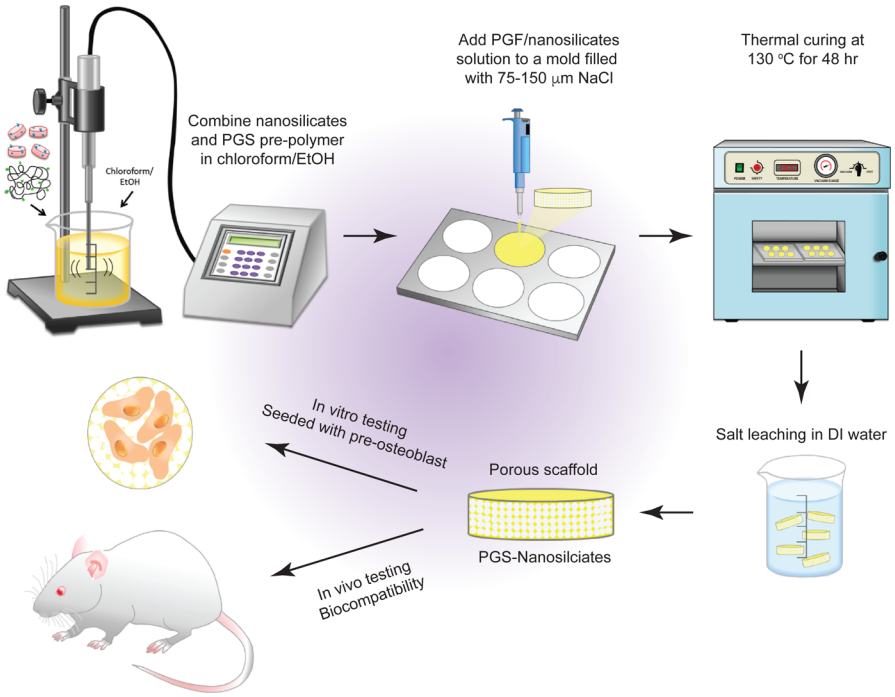

Figure 1. Fabrication of porous nanocomposites scaffolds. PGS-nanosilicates (nSi) scaffolds were fabricated via salt leaching technique. PGS prepolymer mixed with nanosilicates was added to salt-filled (75−150 μm) Teflon molds. Thermal curing at 130°c for 48 h yielded fully cross-linked PGS/nanosilicates networks. Samples were then submerged in deionized water for salt leaching. Porous scaffolds were used for structural, mechanical, and biological characterization.

plate or TCP here) were used as positive controls, and nonseeded TCP as negative controls.

For cell adhesion study, the scaffolds were first glued to a glass slide using silicone sealant to minimize scaffold handling. Preosteoblasts were seeded at 1×10^5 cells in 5 μL normal media per well on the scaffolds. After 3-h incubation, additional 600 μL of normal growth media was added. After 24 h, normal media was replaced by osteoconductive media (α-MEM + 10 mM β-glycerophosphate + 0.05 mM ascorbic acid) in selected wells. Cell culture media was changed every 3 days. The samples were collected after 7 days in culture and prepared for SEM imaging. Samples were gently washed thrice with DPBS before being fixed with 2.5% glutaraldehyde (Alfa Aesar). Then, the samples were dehydrated using an ascending series of ethanol: 30, 50, 75, 95, and 100%, in order. Dehydrated samples were chemically dried using hexamethyldisilazane (HDMS) (electronic grade, Alfa Aesar). The samples were left overnight in a fume hood to allow HDMS to completely evaporate. They were then mounted onto stubs, sputter coated, and imaged.

In Vitro Cell Proliferation and Differentiation. Preosteoblasts were trypsinized at 70% confluency in culture and seeded on pretreated scaffolds at approximately 5000 cells/100 μL of media. Cell proliferation was assessed using alamarBlue assay (Thermo Scientific). The proliferation data was collected on days 1, 3, 5, 7, 10, 14 after the initial cell seeding. Osteogenic differentiation was assessed by investigating alkaline phosphatase (ALP) activity and matrix mineralization. Specifically, after 7 days in culture, the scaffolds were stained with BCIP/NBT substrate solution (Thermo Scientific) for ALP. The stained samples were imaged using a steromicroscope. Moreover, SensoLyte *p*NPP Alkaline Phosphatase Assay Kit was used to quantify ALP activity. ALP activity was then normalized to dsDNA content for each sample. PicoGreen dsDNA quantitation assay (PicoGreen kit, Thermo Scientific) was performed using NanoDrop 3300 fluorospectrometer. In addition, mineralization was assessed by Alizarin Red S (ARS) (2% solution, pH 4.2, Electron Microscopy Science) staining and quantification after 14 days in culture. Before staining, the samples were fixed with 2% glutaraldehyde, and then washed with excess DI water. ARS solution was added for 2 min. The samples were washed with excess DI water again before imaging. For quantification, 10% acetic acid (Fisher Scientific) was added to the stained samples under agitation for 30 min. The ARS-containing acetic acid was collected and neutralized with 10% ammonium hydroxide (Sigma-Aldrich) until the pH was 4.1−4.5. It was then read with a UV/vis plate reader at OD_{405}. Absorbance-ARS concentration conversion was done using a preplotted standard curve.

In Vivo Study in Mice. Biocompatibility, biodegradability, and bioactivity of the scaffolds were studied in vivo. Eight-week-old nonimmunodeficient male BALB/c mice were from Charles River. The animals were handled according to IACUC guidelines (Calabrodental Clinic, 88900 Crotone, Italy). Before operation, they were subjected to an intraperitoneal injection of Ketamin/xilezin (1 mL/kg of 10 mg/mL mixed solution) anesthetic. PGS-10%nSi scaffolds were implanted in the left limb between a long bone and the associated muscle. Briefly, a pocket was created in the connective tissue between the femur and the adductor muscle. The scaffolds (2 × 4 mm) were inserted in the pocket, parallel to the femur bone, and transplanted in triplicate. The mice were hosted in standard conditions, and sacrificed after 3 days, 6 days, and 3 weeks by cervical dislocation. Histology and histochemical analysis were performed on dissected grafts. The dissected grafts were embedded in tissue freezing medium (Leica, Wetzlar, Germany), and then frozen in cool isopropane. Lyica cryostat was used to obtain transverse cryosections of 7 μm. The sections were then strained with hematoxylin and eosin (H&E), toluidine blue, immunofluorescence, and alkaline phosphatase. Axioscop2 plus system equipped with Axicam HRc (Zeiss, Oberkochen, Germany) was used to take images. To quantify the fluorescence signal of the inflammatory cells within the scaffolds, we quantified the IF staining for CD206 by means of ImageJ software (https://imagej.nih.gov/ij/); data were expressed as integrated density, following the subtraction of the background autofluorescence.

Statistics. The data was presented as mean ± standard deviation (n = 3−5). Statistical analysis was performed by one-way analysis of variance (ANOVA) with Turkey's post hoc test for pairwise comparison. Statistical significance designated with $^*p < 0.05$, $^{**}p < 0.01$, and $^{***}P < 0.001$.

DOI: 10.1021/acsbiomaterials.7b00029
ACS Biomater. Sci. Eng. 2017, 3, 590−600

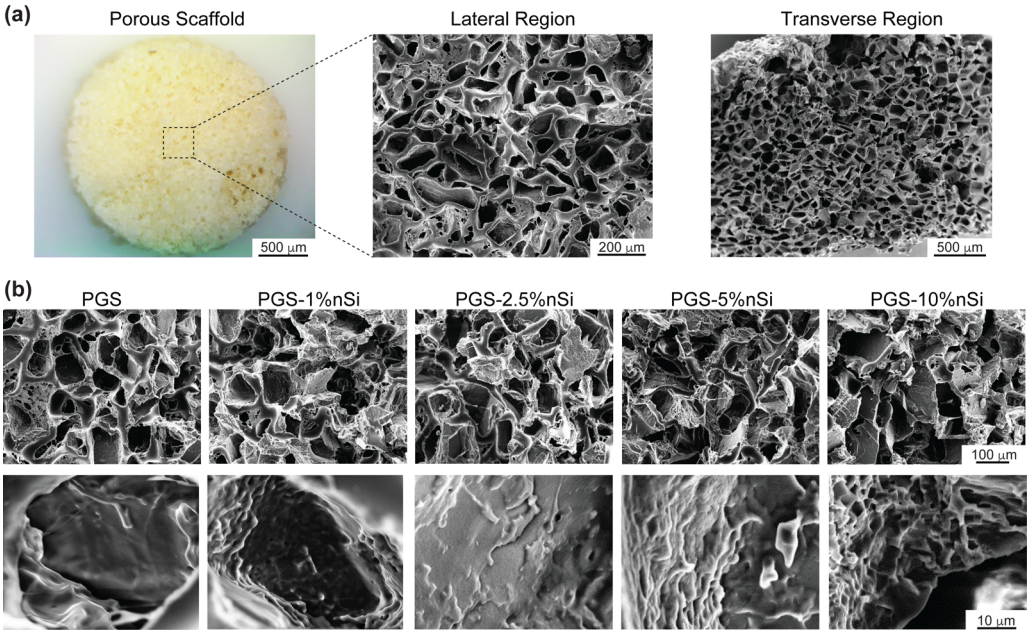

Figure 2. Porous structure of nanocomposite scaffolds. (a) Nanocomposite scaffolds showed highly porous morphology in both lateral and transverse directions. (b) All the scaffolds had a porous microstructure with pore sizes between 75 and 150 μm. High-magnification images showed that the roughness of the pore walls increased with an increase in nanosilicate concentration.

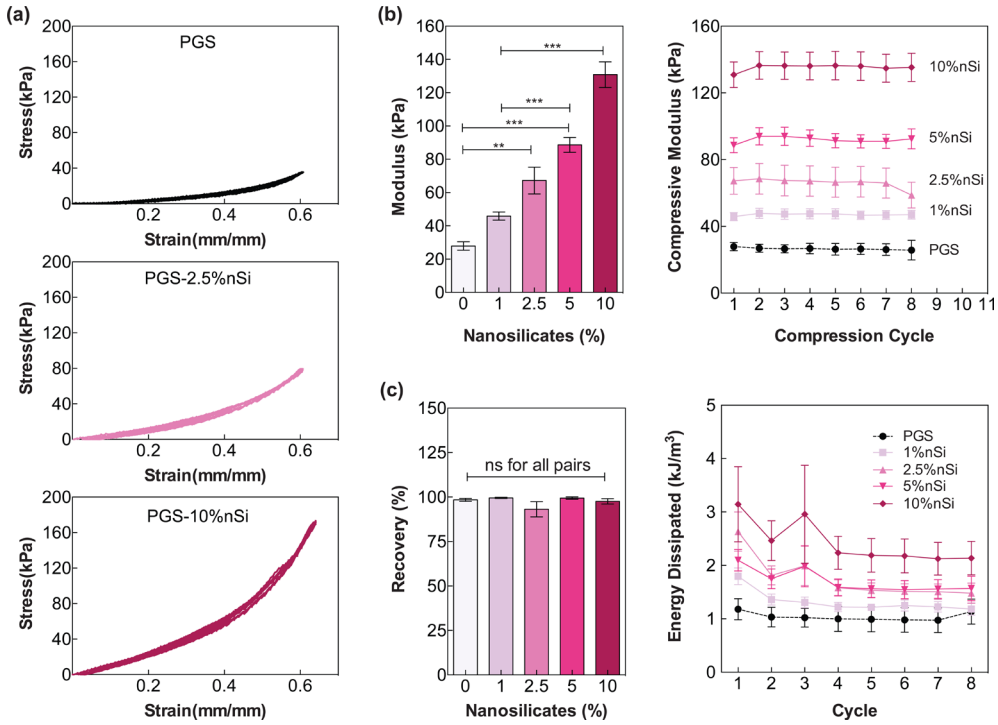

Figure 3. Elastomeric characteristic of nanocomposite scaffolds. (a) Stress−strain curves from cyclic compression testing. Complete recovery of the scaffolds was observed. (b) The compressive modulus increased with an increase in nanosilicate concentration. No change in modulus was observed when the scaffolds were subjected to repeated cyclic compression. (c) Because of their elastomeric nature, all scaffolds showed nearly 100% recovery. The energy absorbed during a cycle was calculated by determining the area within a hysteresis loop. No significant change in energy dissipation was observed during the 8 compressive cycles. The modulus and toughness drastically increased upon the addition of nanosilicates, whereas the elastomericity was not traded off.

■ RESULTS AND DISCUSSION

Porous PGS and PGS-nanosilicates scaffolds were fabricated via salt-leaching method (Figure 1). Nanosilicates and PGS prepolymer were mixed in ethanol/chloroform (3:7) solvent using a probe sonicator. Then, the solution was added to salt-filled Teflon molds. Salt (NaCl) was sieved to obtain particle sizes between 75 and 150 μm. Earlier studies have shown that pore size of ∼100 μm are appropriate to facilitate cell migration and proliferation within a scaffold structure.[42,43] Thermal curing at 130 °C for 48 h yielded fully cross-linked PGS networks from

DOI: 10.1021/acsbiomaterials.7b00029
ACS Biomater. Sci. Eng. 2017, 3, 590−600

PGS prepolymer. These cross-linked samples were then submerged in deionized water for salt leaching and to obtain porous scaffolds. Porous scaffolds were used to evaluate the structural, mechanical, and physiological characteristics. In vitro cell studies and in vivo experiments were also performed to evaluate their efficacy for tissue engineering applications.

Porous Microstructure of PGS/Nanosilicates Scaffolds. The microstructure of salt-leached PGS and PGS-nanosilicate scaffolds was investigated using electron microscopy. The surface (lateral region) of PGS scaffolds displayed porous networks (Figure 2a). The pore size ranged between 75 and 150 μm as designed by the size of NaCl porogens. In addition, smaller micropores with the size of approximately 5−20 μm were distributed between the macropores (75−150 μm). It was likely that the micropores were generated during the curing process. Thermal curing of PGS involved trans-esterification reaction.[44] This led to covalent cross-linking between polymer chains that resulted in 3D network of random coils, turning the viscous liquid into solid elastomer. The solvent and air bubbles were unlikely to be the sources of micropores as chloroform and ethanol are both highly volatile and solvent evaporation was performed under vacuum desiccation for at least 24 h before curing to eliminate air bubbles. In addition, cross-section (transverse region) images showed that the pores were homogeneously distributed across the width and depth of the scaffolds. The morphology of pores present on the scaffold surface and interior appeared to be similar, indicating a uniform microporous network.

The microstructures of PGS and PGS-nanosilicate scaffolds also show a porous network (Figure 2b). The pore size was similar among different scaffolds, suggesting that nanosilicate concentrations had no effect on pore size. This was expected, because the pore size was mainly controlled by NaCl porogens. We could account this as an advantage of the salt-leaching method in comparison to other fabrication techniques; the resultant porous structure could be better controlled and was tunable independent of the scaffold composition. High-magnification images showed that the pore walls of PGS scaffolds were relatively smooth, and the roughness increased upon the addition of nanosilicates. The increase in surface roughness could be attributed to the presence of nanosilicates and their interactions with PGS matrix. It was hypothesized that the rough topography would enhance cell adhesion and spreading.

Nanosilicates Increased Mechanical Stiffness without Compromising Elastomeric Properties. Bone is a dynamic tissue and applied loads play vital roles in determining the rate of turnover as well as the formation of callus, its volume, and stiffness during bone healing. It was reported that scaffolds possessing some elasticity provided a load-transducing environment in which matrix deposition, new bone formation, and maturation could take place.[38] PGS is elastomeric and reinforcing it with nanosilicates is expected to increase its strength and toughness.

Mechanical characteristics of the scaffolds were investigated using uniaxial cyclic compression (8 cycles). All samples (both PGS and PGS/nanosilicates) exhibited nonlinear stress−strain behavior (Figure 3a), which is typical for elastomeric materials. From the stress−strain curves, compressive modulus, recovery, and energy dissipation were determined. The results showed that the addition of nanosilicates significantly increased the compressive modulus of nanocomposites in a concentration-dependent manner (Figure 3b). The compressive modulus for the scaffolds containing 0, 1, 2.5, 5, and 10% nanosilicates were 27.9 ± 5.1 kPa, 45.9 ± 4.8 kPa, 67.2 ± 16.1 kPa, 88.6 ± 9.0 kPa, and 130.8 ± 15.3 kPa, respectively. The addition of 10% nanosilicates to PGS enhanced the modulus 4.5-fold compared to PGS scaffolds. This could be because nanosilicates interacted strongly with PGS, restraining polymer chain movement as well as improving load transfer capability during deformation. In this regard, nanosilicates were reported to drastically improve mechanical properties of soft nanocomposites.[28,45] We did not observe any significant change in modulus when samples were subjected to multiple compressive cycles (1−8 cycles).

To evaluate the elastomeric characteristics of nanocomposites we evaluated energy dissipation during each cycle (Figure 3c). The first cycle displayed maximum energy absorption. It then decreased and remained rather unchanging during subsequent cycles for all scaffold compositions. For example, PGS-1%nSi scaffolds absorbed 1.8 ± 0.3 kJ/m^3 during cycle 1 and approximately 1.3 ± 0.2 kJ/m^3 during cycles 2−8. Moreover, the addition of nanosilicates did not compromise elasticity of scaffolds, as indicated by increased energy dissipation with increasing nanosilicate concentrations. During the first cycle, the scaffolds with 0, 1, 2.5, 5, and 10% nanosilicates absorbed 1.2 ± 0.4, 1.8 ± 0.3, 2.6 ± 0.8, 2.1 ± 0.4, and 3.1 ± 1.6 kJ/m^3, respectively. We observed that the addition of 10% nanosilicates to PGS network resulted in >2.5 times increase in energy dissipation. Our previous studies showed that the addition of 10% nanosilicates to solid PGS/nanosilicates nanocomposites gave rise to over 6.5 times increase in energy dissipation.[40] Because the porous structure of the scaffolds was controlled by porogens, it is likely that the effects of nanosilicates were less in comparison to their nonporous counterparts.

Recovery of cross-linked network after cyclic mechanical deformation was calculated from the stress−strain curves. PGS network consisted of random coils that are covalently linked with one another. The hydrogen bonding between −OH groups of the PGS backbone contributed to the observed elastomeric characteristics.[35,46] Interestingly, the addition of nanosilicates did not compromise elasticity of the scaffolds despite enhancing strength and elasticity. In particular, nanosilicate concentration did not have statistically significant effects on network recovery (Figure 3c). For example, after 8 cycles of compression, recovery of PGS and PGS-10%nSi scaffolds was found to be 98.4 ± 1.4% and 97.6 ± 3.4%, respectively. These results suggested that mechanical properties of PGS/nanosilicates scaffolds were tunable. The addition of nanosilicates increased mechanical strength, while maintaining their elastomeric properties. This would be beneficial as some flexibility is required in the early stage of fracture repair involving cartilage formation prior to bone calcification[47] In the future, we aim to increase nanosilicate concentration or cross-linking density of the PGS network to bring the mechanical properties closer to those of cancellous bone. Earlier studies have shown that nanocomposites containing 70% nanosilicates are cytocompatible.[48] Another option to increase the mechanical stiffness is to decrease pore size of the scaffold or to incorporate crystalline polymer. Considering the achieved mechanical properties, it is promising that PGS/nanosilicates scaffolds could be used for craniofacial defects.

Nanosilicates Enhanced Physiological Stability of the Scaffolds. It is well established that the degradation profile of scaffolds is profoundly important to how they perform. Scaffolds should give structural support and at the same time allow gradual replacement with newly formed bone. Under physiological conditions, PGS undergoes surface erosion via cleavage of ester

DOI: 10.1021/acsbiomaterials.7b00029
ACS Biomater. Sci. Eng. 2017, 3, 590−600

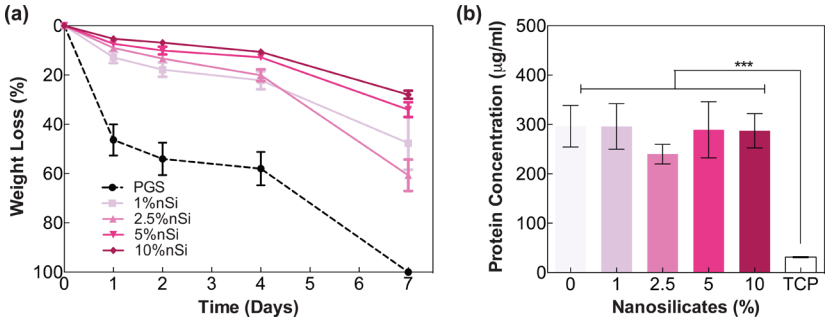

Figure 4. Physiological characteristics of nanocomposite scaffolds. (a) Effects of nanosilicates on physiological stability of the scaffolds were evaluated in accelerated degradation conditions (0.01 M NaOH solutions) over a week. PGS degraded completely via hydrolytic degradation within a week, while the addition of 10% nanosilicates resulted in ∼30% weight loss. Nanosilicates greatly improved physiological stability of the scaffolds. (b) The addition of nanosilicates had insignificant effects on protein adsorption. The amount of protein adsorbed on the scaffolds was significantly higher than that on TCP controls. This could be due to combinatorial effects of porosity and surface properties of the scaffolds.

bonds.[36] From a tissue engineering standpoint, surface-eroding polymers are preferred over bulk-degrading ones since they can maintain more linear reduction in structural integrity and mechanical performance as mass loss continues over time. In preliminary studies, scaffold degradation was studied for 1 week in PBS, 37 °C. Less than 3% weight loss was observed for all samples (data not shown). With standard deviation taken into account, the differences between compositions were statistically inconclusive. Under in vivo conditions, PGS degrades in approximately 35−50 days.[36] To accelerate the degradation to fewer days, we carried out accelerated degradation tests using 0.01 M NaOH solution. Basic condition was used to accelerate the process (7−10 days), and it was anticipated that the trends would be more prominent.

Percentage of weight loss was measured on days 1, 2, 4, and 7. The addition of nanosilicates (1, 2.5, 5 and 10%) was found to significantly reduce weight loss compared to PGS scaffolds (Figure 4a). For example, after 1 week, PGS scaffolds were completely degraded, whereas nanocomposite scaffolds loaded with 1%, 2.5%, 5%, and 10% nanosilicates showed 47.7 ± 24.4, 60.7 ± 14.2, 34 ± 6.6, and 28 ± 3.4% weight loss, respectively. That means more than 3.5 times reduction in weight loss upon the addition of 10% nanosilicates. Although, we observed a reduction in weight loss due to nanosilicate addition, but there was no significant difference between nanocomposites containing 1% and 2.5% nanosilicates. This might be attributed to a significantly low amount of nanosilicates compared to PGS. The increases in physical integrity with the addition of nanosilicates could be observed for all studied time points. In addition, the scaffolds remained intact and maintained their shape upon degradation, i.e., they became smaller disks over time. This indicated a surface eroding nature, which was beneficial because the scaffolds would be able to better maintain their structural integrity during new tissue regeneration in comparison to bulk degrading scaffolds.

It has been demonstrated that degradation kinetics of PGS could be entirely altered by varying degree of cross-linking. In this case, nanosilicates acted as cross-linkers, retarding degradation of the polyester backbone resulting in enhanced physical integrity. Our previous studies showed that cross-linking density of thermally cured PGS/nanosilicates nanocomposites was increased upon the addition of nanosilicates.[40] Sol−gel analysis was used to investigate degree of covalent cross-linking in that study. The sol (un-cross-linked) fraction was statistically significantly reduced with increasing nanosilicate concentrations. The results agreed with other published works that nanosilicates could serve as multifunctional cross-linkers.[45,49] It is anticipated that the cross-linking involved transesterification with the secondary alcohol of glycerol. Nevertheless, the exact nature of cross-linking mechanisms will need further investigation.

PGS degrades by hydrolysis of esters while nanosilicates slowly disintegrate at pH <9. Short-term degradation of the scaffolds was dominated by PGS hydrolysis. To get a more complete degradation profile, long-term (months) studies that take nanosilicate disintegration into account will need to be performed. The results shown here demonstrated the effects of nanosilicates on scaffold degradation, and that it was tailorable, but they did not represent the actual time frame of degradation. Noteworthy, it was reported that PGS degraded faster in vivo than in vitro due to presence of esterase in body.[50]

PGS/Nanosilicates Scaffolds Were Protein Adhesive. When the scaffolds come into contact with physiological mediums, it is believed that the initial event is protein adsorption. The adsorbed protein layer will influence the subsequent biological responses including cell adhesion and migration.[51] As proteins are viewed as primary players in mediating material-cell interactions, protein adsorption on PGS/nanosilicates scaffolds was investigated along with the cellular studies. Fetal bovine serum (FBS) was used for protein adsorption studies as it is a component of cell culture media. After 24 h, concentration of FBS adsorbed on the scaffold surface was measured using micro BCA assay. The results showed that protein adsorption on the scaffolds was significantly higher than that on TCP control, and there was no statistically significant difference between scaffold compositions (Figure 4b). On average, proteins adsorbed on the scaffolds were approximately 9 times higher than that on TCP. This might have been expected because porous scaffolds had a greater surface area than TCP. Nevertheless, our previous studies with nonporous PGS/nanosilicates nanocomposites revealed that protein adsorption on the nanocomposite's surface was twice that on TCP.[40] Considering that the effects of nanosilicates on protein adsorption were statistically insignificant, it was likely that surface properties of PGS itself could promote protein adsorption.

PGS/Nanosilicates Scaffolds Enhanced Cell Adhesion and Supported Cell Proliferation. The scaffolds seeded with MC-3T3 preosteoblasts were imaged with SEM in order to investigate cell adhesion and morphology. All scaffolds (both PGS and PGS/nanosilicates) were found to support cell adhesion well. Remarkably, an increase in cell spreading was observed due to the addition of nanosilicates; more pronounced effects were observed on the scaffolds cultured in normal growth

DOI: 10.1021/acsbiomaterials.7b00029
ACS Biomater. Sci. Eng. 2017, 3, 590−600

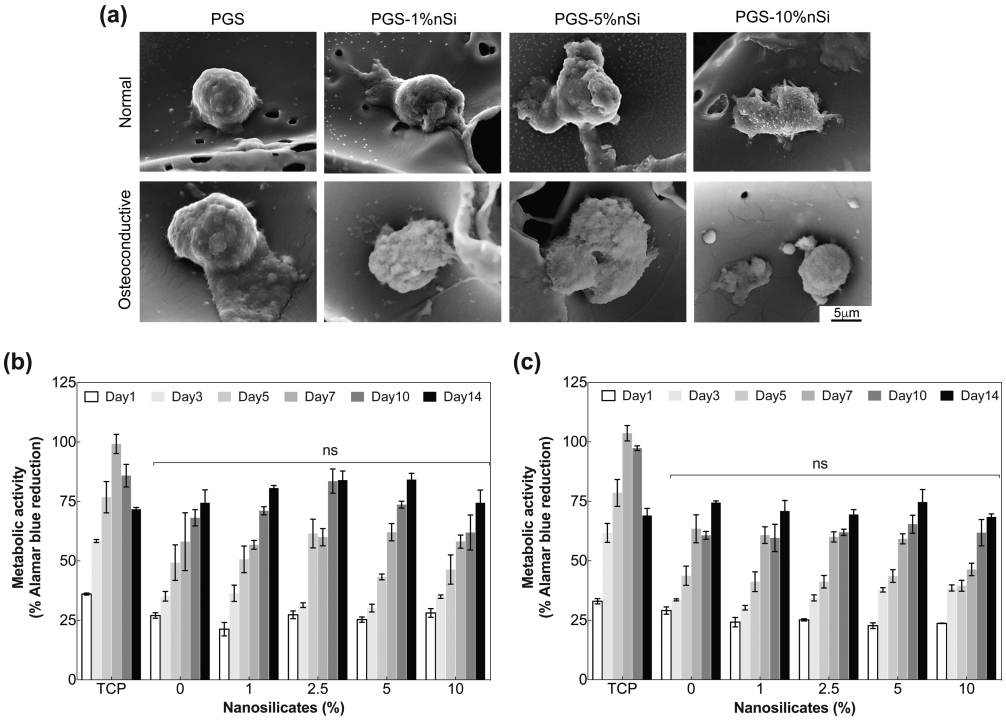

Figure 5. In vitro evaluation of porous nanocomposite scaffolds. (a) SEM images of preosteoblasts after 7 days in culture showed well-adhered cells on the scaffolds. Cell adhesion and spreading increased with increasing nanosilicate concentration. (b, c) Metabolic activty of adherent cells was determined over a period of 2 weeks. There was no significant change in cell proliferation upon the addition of nanosilicates and in different media compositions.

media in comparison with in osteoconductive media (Figure 5a). This might be attributed to the presence of nanosilicates or enhanced surface stiffness, or both. Previous works from our research group demonstrated that incorporation of nanosilicates to cell-resistant and antifouling substrates (poly(ethylene)glycol (PEG)) greatly increased cell adhesion as well as cell spreading in a concentration-dependent manner.[48−50,52] In those studies, it was hypothesized that nanosilicates served as protein adsorption sites which subsequently promoted cell adhesion. This might controvert the results showing that the effects of nanosilicates on the number of proteins adsorbed on the scaffolds were statistically insignificant (Figure 4b). Nevertheless, the actual mechanisms underlying increased cell spreading with increasing nanosilicate concentrations are still unclear. Furthermore, increased cell spreading has been reported to promote osteogenic differentiation while suppressing adipogenic differentiation of mesenchymal stem cells (MSCs). This could be due to enhanced cytoskeletal contractility with increased cell spreading, as high contractility was found to correlate with osteogenesis.[40,53] Thus, we hypothesized that the enhanced cell spreading on PGS/nanosilicates scaffolds would favor osteogenic differentiation.

Metabolic activity of seeded preosteoblasts was studied over 2 weeks using AlamarBlue assay (Figure 5b, c). All PGS and PGS-nanosilicates scaffolds were found to support cell proliferation. Metabolic activity of the cells increased over time, except for TCP, on which the activity started to decrease after 10 days. The decline could be attributed to the cells reaching confluency, which was not observed on the scaffolds possessing higher surface area. There was no statistically significant difference in cell proliferation between scaffold compositions, and the trends were the same for both culture mediums. The results suggested cytocompatibility of nanosilicates as well as the scaffolds. As mentioned earlier, nanosilicates were reported to be cytotoxic at a 10-fold higher concentration as compared with silica nanoparticles and the widely used nanohydroxyapatite.[17] Also, PGS is biocompatible and its degradation products are often metabolized in the body.[35]

AlamarBlue assay showed that effects of nanosilicates on preosteoblast proliferation were insignificant. The results disagreed with a previous work reporting increased cell proliferation on poly(ethylene oxide) (PEO)/nSi substrates with increasing nanosilicate concentrations.[48] This could be explained by the fact that PEO surface was low cell-adherent such that the increases in cell metabolic activity as a result of nanosilicate incorporation were significant, whereas PGS innately promoted cell adhesion and proliferation. Particularly, cell proliferation on PGS solid substrates was found to be slightly slower than that on TCP, whereas metabolic activity of cells on PEO-nanosilicate systems was still significantly lower than that on TCP even with addition of 70% nanosilicates.[54]

Cross-section SEM images of the seeded scaffolds after 7 days in culture revealed limited cell migration down the pores (data not shown). After thorough inspection, limited pore connectivity was likely to be the cause. This could be improved by particulate fusion method where the porogens would be fused together in a humidity chamber before used as a template for solvent casting. This fabrication technique should create a more open porous structure. The extensive micropores resulting from salt-fusion should increase mass transfer as well as cellular communication, and facilitate the formation of a 3D tissue construct.

PGS/Nanosilicates Scaffolds Promoted Osteogenic Differentiation. Osteogenic differentiation of preosteoblasts seeded on the scaffolds was investigated by assessing alkaline phosphatase (ALP) activity and matrix mineralization. ALP activity, an early hallmark indicator of osteogenic differentiation, was examined after 7 days in culture. Our results showed that PGS was osteoconductive and preosteoblasts seeded on PGS

DOI: 10.1021/acsbiomaterials.7b00029
ACS Biomater. Sci. Eng. 2017, 3, 590−600

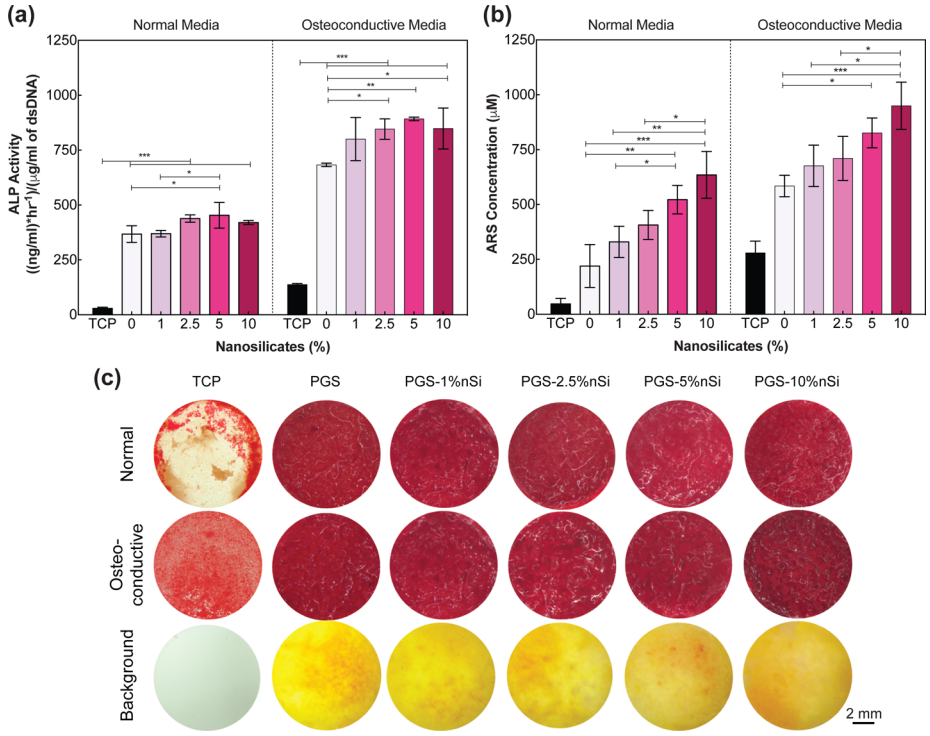

Figure 6. In vitro bioactivity of porous nanocomposite scaffolds. (a) Preosteoblast seeded on PGS scaffolds showed enhanced ALP activity compared to TCP controls. The addition of nanosilicates to PGS also gave rise to significant enhancement in ALP activity. A similar trend was observed in osteoconductive media. (b, c) Formation of mineralized matrix is a hallmark of osteogenic differentiation. After 14 days in culture, cells seeded on TCP controls and nanocomposite scaffolds were stained using Alizarin Red S (ARS) to visualize mineralized matrix (strained red). The images showed formation of mineralized matrix on all PGS and PGS-nSi scaffolds. Quantification of ARS indicated that the mineralization increased with an increase in nanosilicate concentration, in both normal and osteconductive media.

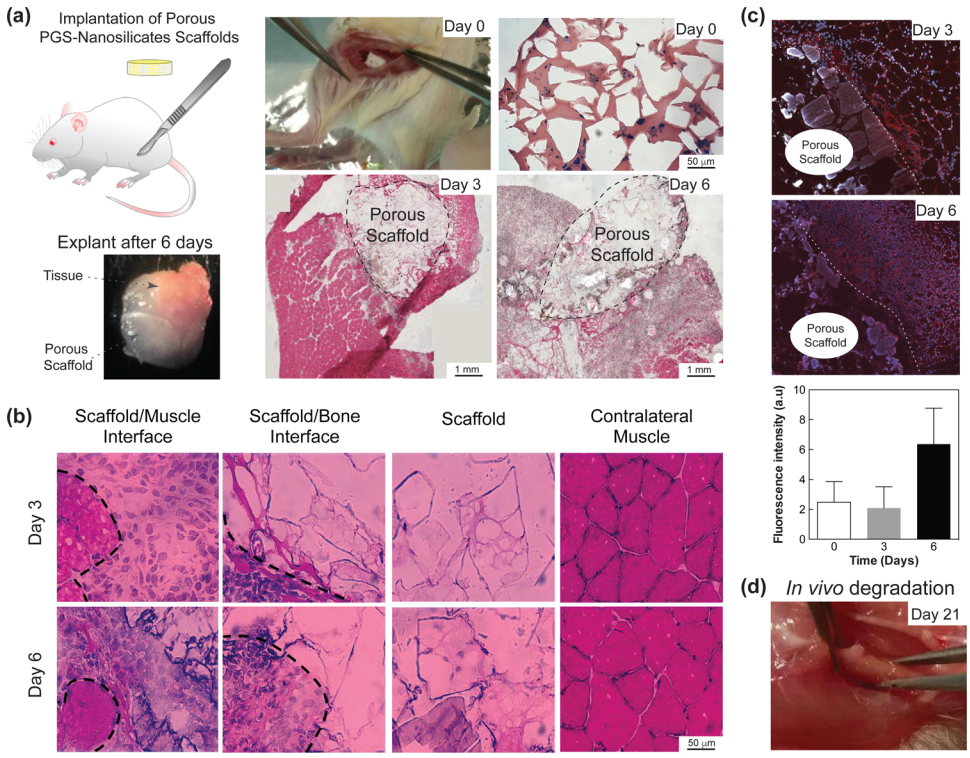

Figure 7. In vivo biocompatibility of nanocomposite scaffolds. (a) PGS-nSi scaffolds were implanted in the intramuscular region and harvested after 3 and 6 days. (b) H&E staining of the explants indicated cellular infiltration within the scaffolds. (c) High-magnification images revealed inflammatory infiltration at the scaffold/muscle and scaffold/bone interface, at both 3 and 6 days. (d) After 21 days, degradation of the scaffolds was observed without signs of inflammation, indicating biodegradable characteristics.

DOI: 10.1021/acsbiomaterials.7b00029
ACS Biomater. Sci. Eng. 2017, 3, 590−600

scaffolds were stained for ALP. Our results supported earlier observation that PGS scaffolds are osteoconductive and support production of mineralized extracellular matrix from seeded osteoblasts.[40,55−57] The addition of nanosilicates to PGS significantly enhanced the ALP activity of seeded preosteoblast cells. Quantitative analysis of ALP/dsDNA showed that nanosilicates enhanced ALP activity; the enhancement was more prominent in osteoconductive media than in normal growth media (Figure 6a). It should be noted that the increases could be seen even when the scaffolds were cultured in the media without any osteogenic supplements.

After 14 days in culture, the scaffolds were stained using Alizarin Red S (ARS) to determine presence of mineralized matrix. ARS quantification clearly showed increased matrix mineralization upon the addition of nanosilicates in a concentration-dependent manner (Figure 6b). The enhancement was apparent in both normal growth media and osteconductive media. For example, the addition of 10% nanosilicates gave rise to an almost 3-fold increase in normal growth media and over 1.5-fold increase in osteoconductive media. For all scaffold compositions, degree of osteogenic differentiation was higher in osteoconductive media than in normal growth media as expected. All scaffolds were stained bright red with ARS (Figure 6c). However, because they were all highly stained, the differences between compositions could not be observed from the images. Remarkably, these results indicated nanosilicates's critical roles in upregulating osteogenic differentiation. The apparent increases in ALP activity and matrix mineralization when cultured in normal growth media suggested osteoinductive properties of nanosilicates as previously reported. The osteoinductive capability of nanosilicates offers a growth-factor-free approach for bone regeneration that could minimize the expense and complexity involved in growth factor delivery.

In Vivo Biocompatibility, Biodegradability, and Bioactivity. In vivo biocompatibility of PGS-nanosilicates scaffolds was investigated by intramuscular implantation. The scaffolds were implanted between the femur bone and the quadriceps (Figure 7a). Nanocomposite scaffolds were harvested after 3 and 6 days following implantation. The scaffolds were dissected and stained with H&E. Their structure and composition were conserved. Porous networks of nanocomposite scaffolds were clearly visible. Major and minor axes of the pores were measured to be 105 ± 6 and 72 ± 5 μm, respectively, which agreed with the SEM images (Figure 2b). H&E images showed the scaffold/bone interface at the top and scaffold/muscle interface at the bottom; the muscle bundles were clearly evident. The scaffolds appeared porous with brownish nanosilicate crystals. High-magnification images revealed inflammatory infiltration at the scaffold/muscle and scaffold/bone interface, at both 3 and 6 days (Figure 7b, c). Inflammatory cells were seen within the scaffolds at 6 days but not 3d. Contralateral, mocked operated muscles were used as controls. No inflammatory infiltration was seen in the controls, indicating that the observed inflammatory responses were triggered by the scaffolds and not by the grafting procedures. It also suggested that the presence of the scaffolds did not induce generalized inflammation in all muscles. These data were also confirmed by the quantification of the immunofluorescence signal related to CD206, where the fluorescence intensity at 3 and at 0 days (control on the contralateral femur bone/quadriceps muscle) was significantly lower with respect to the data at 6 days. At 21 days following implantation, the mice were healthy and showed no sign of distress. Upon dissection, no major sign of inflammation (e.g., edema) was observed. After 21 days, scaffolds showed signs of degradation, indicating biodegradability of nanocomposites (Figure 7d). Overall, in vivo studies indicated biocompatibility of nanocomposites scaffolds and thus they are promising for bone tissue engineering.

■ CONCLUSIONS

We successfully fabricated porous nanocomposite scaffolds of PGS/nanosilicates. The addition of nanosilicates gave rise to enhanced physical integrity as well as increased mechanical strength and toughness, whereas it did not compromise elastomericity, the mechanical characteristic that would provide a load-transducing environment for bone regeneration. The achieved mechanical properties looked promising for craniofacial defect reconstruction. In the future, we aim to increase nanosilicate contents to obtain compressive modulus and toughness closer to that of trabecular bone. The scaffolds supported preosteoblast proliferation and increased cell adhesion and spreading into the morphology reported to favor osteogenic differentiation. PGS/nanosilicates scaffolds could promote osteogenic differentiation without any osteogenic supplements, suggesting their osteoinductive capability. Moreover, the nanocomposite scaffolds were biocompatible, biodegradable, and did not induce persistent inflammation in vivo. Overall, the results have demonstrated the potential of PGS/nanosilicates scaffolds for growth factor-free bone tissue engineering.

■ AUTHOR INFORMATION

Corresponding Author

*E-mail: gaharwar@tamu.edu. Telephone: (979) 458-5540. Fax: (979) 845-4450.Address: 3120 TAMU, 5024 Emerging Technology Building, College Station, TX 77843-3120.

ORCID

Akhilesh K. Gaharwar: 0000-0002-0284-0201

Author Contributions

P.K. and A.K.G. conceptualized the idea and designed the project. P.K., M.K., and P.J. performed physical and chemical characterization. P.K. performed and analyzed in vitro cellular studies, whereas M.T. and B.P. performed and analyzed in vivo work. P.K. and A.K.G. analyzed the results and wrote the manuscript. All authors contributed in revising the manuscript.

Notes

The authors declare no competing financial interest.

■ ACKNOWLEDGMENTS

A.K.G. acknowledges funding support from Texas Engineering Experiment Station and Texas A&M University Seed Grant.

■ REFERENCES

(1) Giannoudis, P. V.; Dinopoulos, H.; Tsiridis, E. Bone Substitutes: An Update. *Injury, Int. J. Care Injured* **2005**, *36*, S20−S27.

(2) Grabowski, G.; Cornett, C. A. Bone Graft and Bone Graft Substitutes in Spine Surgery: Current Concepts and Controversies. *Journal of the American Academy of Orthopaedic Surgeons* **2013**, *21* (1), 51−60.

(3) Pape, H. C.; Evans, A.; Kobbe, P. Autologous Bone Graft: Properties and Techniques. *Journal of Orthopaedic Trauma* **2010**, *24* (3), S36−S40.

(4) Marino, J. T.; Ziran, B. H. Use of Solid and Cancellous Autologous Bone Graft for Fractures and Nonunions. *Orthopedic Clinics of North America* **2010**, *41* (1), 15−26.

(5) Kneser, U.; Schaefer, D. J.; Polykandriotis, E.; Horch, R. E. Tissue Engineering of Bone: The Reconstructive Surgeon's Point of View. *J. Cell. Mol. Med.* **2006**, *10* (1), 7−19.

DOI: 10.1021/acsbiomaterials.7b00029
ACS Biomater. Sci. Eng. 2017, 3, 590−600

(6) Bohner, M. Resorbable Biomaterials as Bone Graft Substitutes. *Mater. Today* **2010**, *13* (1−2), 24−30.
(7) Greenwald, A. S.; Boden, S. D.; Goldberg, V. M.; khan, Y.; Laurencin, C. T.; Rosier, R. N. Bone-graft Substitutes: Facts, Fictions, and Applications. *J. Bone Jt. Surg.* **2001**, *83*, 98−103.
(8) Blokhuis, T. J.; Arts, J. J. C. Bioactive and Osteoinductive Bone Graft Substitutes: Definitions, Facts and Myths. *Injury* **2011**, *42* (Suppl 2), S26−S29.
(9) Jones, J. R. Review of Bioactive Glass: From Hench to Hybrids. *Acta Biomater.* **2013**, *9*, 4457−4486.
(10) Seebach, C.; Schultheiss, J.; Wilhelm, K.; Frank, J.; Henrich, D. Comparison of Six Bone-graft Substitutes Regarding to Cell Seeding Efficiency, Metabolism and Growth Behaviour of Human Mesenchymal Stem Cells (MSC) In Vitro. *Injury* **2010**, *41* (7), 731−738.
(11) Valliant, E. M.; Jones, J. R. Softening Bioactive Glass for Bone Regeneration: Sol−gel Hybrid Materials. *Soft Matter* **2011**, *7*, 5083−5095.
(12) Moore, W. R.; Graves, S. E.; Bain, G. I. Synthetic Bone Graft Substitutes. *ANZ. J. Surg.* **2001**, *71*, 354−361.
(13) Gaharwar, A. K.; Peppas, N. A.; Khademhosseini, A. Nanocomposite Hydrogels for Biomedical Applications. *Biotechnol. Bioeng.* **2014**, *111* (3), 441−453.
(14) Carrow, J. K.; Gaharwar, A. K. Bioinspired Polymeric Nanocomposites for Regenerative Medicine. *Macromol. Chem. Phys.* **2015**, *216* (3), 248−264.
(15) Cross, L. M.; Thakur, A.; Jalili, N. A.; Detamore, M.; Gaharwar, A. K. Nanoengineered biomaterials for repair and regeneration of orthopedic tissue interfaces. *Acta Biomater.* **2016**, *42*, 2−17.
(16) Chimene, D.; Alge, D. L.; Gaharwar, A. K. Two-Dimensional Nanomaterials for Biomedical Applications: Emerging Trends and Future Prospects. *Adv. Mater.* **2015**, *27* (45), 7261−7284.
(17) Gaharwar, A. K.; Mihaila, S. M.; Swami, A.; Patel, A.; Sant, S.; Reis, R. L.; Marques, A. P.; Gomes, M. E.; Khademhosseini, A. Bioactive Silicate Nanoplatelets for Osteogenic Differentiation of Human Mesenchymal Stem Cells. *Adv. Mater.* **2013**, *25*, 3329−3336.
(18) Mihaila, S. M.; Gaharwar, A. K.; Reis, R. L.; Khademhosseini, A.; Marques, A. P.; Gomes, M. E. The Osteogenic Differentiation of SSEA-4 Sub-population of Human Adipose Derived Stem Cells Using Silicate Nanoplatelets. *Biomaterials* **2014**, *35*, 9087−9099.
(19) Xavier, J. R.; Thakur, T.; Desai, P.; Jaiswal, M. K.; Sears, N.; Cosgriff-Hernandez, E.; Kaunas, R.; Gaharwar, A. K. Bioactive Nanoengineered Hydrogels for Bone Tissue Engineering: A Growth-Factor-Free Approach. *ACS Nano* **2015**, *9* (3), 3109−3118.
(20) Hoppe, A.; Güldal, N. S.; Boccaccini, A. R. A Review of the Biological Response to Ionic Dissolution Products From Bioactive Glasses and Glass-ceramics. *Biomaterials* **2011**, *32*, 2757−2774.
(21) Zreiqat, H.; Howlett, C. R.; Zannettino, A.; Evans, P.; Schulze-Tanzil, G.; Knabe, C.; Shakibaei, M. Mechanisms of Magnesium-stimulated Adhesion of Osteoblastic Cells to Commonly Used Orthopaedic Implants. *J. Biomed. Mater. Res.* **2002**, *62* (2), 175−184.
(22) Kubota, T.; Michigami, T.; Ozono, K. Wnt Signaling in Bone Metabolism. *J. Bone Miner. Metab.* **2009**, *27*, 265−271.
(23) Reffitt, D. M.; Ogston, N.; Jugdaohsingh, R.; Cheung, H. F. J.; Evans, B. A. J.; Thompson, R. P. H.; Powell, J. J.; Hampson, G. N. Orthosilicic Acid Stimulates Collagen Type 1 Synthesis and Osteoblastic Differentiation in Human Osteoblast-like Cells In Vitro. *Bone* **2003**, *32*, 127−135.
(24) Podsiadlo, P.; Kaushik, A. K.; Arruda, E. M.; Waas, A. M.; Shim, B. S.; Xu, J.; Pumplin, B. G.; Lahann, J.; Ramamoorthy, A.; Kotov, N. A. Ultrastrong and Stiff Layered Polymer Nanocomposites. *Science* **2007**, *318* (5847), 80−83.
(25) Gaharwar, A. K.; Rivera, C. P.; Wu, C.-J.; Schmidt, G. Transparent, Elastomeric and Tough Hydrogels from Poly(ethylene glycol) and Silicate Nanoparticles. *Acta Biomater.* **2011**, *7*, 4139−4148.
(26) Bonderer, L. J.; Studart, A. R.; Gauckler, L. J. Bioinspired Design and Assembly of Platelet Reinforced Polymer Films. *Science* **2008**, *319* (5866), 1069−1073.
(27) Gaharwar, A. K.; Schexnailder, P.; Kaul, V.; Akkus, O.; Zakharov, D.; Seifert, S.; Schmidt, G. Highly Extensible Bio-Nanocomposite Films with Direction-Dependent Properties. *Adv. Funct. Mater.* **2010**, *20*, 429−436.
(28) Haraguchi, K. Synthesis and Properties of Soft Nanocomposite Materials with Novel Organic/inorganic Network Structures. *Polym. J.* **2011**, *43*, 223−241.
(29) Gaharwar, A. K.; Avery, R. K.; Assmann, A.; Paul, A.; McKinley, G. H.; Khademhosseini, A.; Olsen, B. D. Shear-Thinning Nanocomposite Hydrogels for the Treatment of Hemorrhage. *ACS Nano* **2014**, *8* (10), 9833−9842.
(30) Wang, Q.; Mynar, J. L.; Yoshida, M.; Lee, E.; Lee, M.; Okuro, K.; Kinbara, K.; Aida, T. High-water-content Mouldable Hydrogels by Mixing Clay and a Dendritic Molecular Binder. *Nature* **2010**, *463*, 339−343.
(31) Dawson, J. I.; Kanczler, J. M.; Yang, X. B.; Attard, G. S.; Oreffo, R. O. C. Clay Gels For the Delivery of Regenerative Microenvironments. *Adv. Mater.* **2011**, *23*, 3304−3308.
(32) Dawson, J. I.; Oreffo, R. O. C. Clay: New Opportunities for Tissue Regeneration and Biomaterial Design. *Adv. Mater.* **2013**, *25*, 4069−4086.
(33) Waters, R.; Pacelli, S.; Maloney, R.; Medhi, I.; Ahmed, R. P.; Paul, A. Stem cell secretome-rich nanoclay hydrogel: a dual action therapy for cardiovascular regeneration. *Nanoscale* **2016**, *8* (14), 7371−7376.
(34) Paul, A.; Manoharan, V.; Krafft, D.; Assmann, A.; Uquillas, J. A.; Shin, S. R.; Hasan, A.; Hussain, M. A.; Memic, A.; Gaharwar, A. K.; Khademhosseini, A. Nanoengineered Biomimetic Hydrogels for Guiding Human Stem Cell Osteogenesis in Three Dimensional Microenvironments. *J. Mater. Chem. B* **2016**, *4* (20), 3544−3554.
(35) Rai, R.; Tallawi, M.; Grigore, A.; Boccaccini, A. R. Synthesis, Properties and Biomedical Applications of Poly(glycerol sebacate) (PGS): A Review. *Prog. Polym. Sci.* **2012**, *37*, 1051−1078.
(36) Wang, Y.; Kim, Y. M.; Langer, R. In Vivo Degradation Characteristics of Poly(glycerol sebacate). *J. Biomed. Mater. Res.* **2003**, *66A* (1), 192−197.
(37) Wang, Y.; Ameer, G. A.; Sheppard, B. J.; Langer, R. A Tough Biodegradable Elastomer. *Nat. Biotechnol.* **2002**, *20*, 602−606.
(38) Zaky, S. H.; Lee, K.-W.; Gao, J.; Jensen, A.; Close, J.; Wang, Y.; Almarza, A. J.; Sfeir, C. Poly(Glycerol Sebacate) Elastomer: A Novel Material for Mechanically Loaded Bone Regeneration. *Tissue Eng., Part A* **2014**, *20* (1-2), 45−53.
(39) Deng, Y.; Bi, X.; Zhou, H.; You, Z.; Wang, Y.; Gu, P.; Fan, X. Repair of Critical-Sized Bone Defects with Anti-MIR-31-Expressing Bone Marrow Stromal Stem Cells and Poly(glycerol sebacate) Scaffolds. *European Cells and Materials* **2014**, *27*, 13−25.
(40) Kerativitayanan, P.; Gaharwar, A. K. Elastomeric and Mechanically Stiff Nanocomposites from Poly(glycerol sebacate) and Bioactive Nanosilicates. *Acta Biomater.* **2015**, *26*, 34−44.
(41) Patel, A.; Gaharwar, A. K.; Iviglia, G.; Zhang, H.; Mukundan, S.; Mihaila, S. M.; Demarchi, D.; Khademhosseini, A. Highly elastomeric poly (glycerol sebacate)-co-poly (ethylene glycol) amphiphilic block copolymers. *Biomaterials* **2013**, *34* (16), 3970−3983.
(42) Freyman, T.; Yannas, I.; Gibson, L. Cellular materials as porous scaffolds for tissue engineering. *Prog. Mater. Sci.* **2001**, *46* (3), 273−282.
(43) Karageorgiou, V.; Kaplan, D. Porosity of 3D biomaterial scaffolds and osteogenesis. *Biomaterials* **2005**, *26* (27), 5474−5491.
(44) Gao, J.; Crapo, P. M.; Wang, Y. Macroporous Elastomeric Scaffolds with Extensive Micropores for Soft Tissue Engineering. *Tissue Eng.* **2006**, *12* (4), 917−925.
(45) Dawson, J. I.; Oreffo, R. O. C. Clay: New Opportunities for Tissue Regeneration and Biomaterial Design. *Adv. Mater.* **2013**, *25*, 4069−4086.
(46) Gaharwar, A. K.; Patel, A.; Dolatshahi-Pirouz, A.; Zhang, H.; Rangarajan, K.; Iviglia, G.; Shin, S.-R.; Hussain, M. A.; Khademhosseini, A. Elastomeric nanocomposite scaffolds made from poly(glycerol sebacate) chemically crosslinked with carbon nanotubes. *Biomater. Sci.* **2015**, *3*, 46.
(47) Chen, Q.-Z.; Quinn, J. M. W.; Thouas, G. A.; Zhou, X.; Komesaroff, P. A. Bone-Like Elastomer-Toughened Scaffolds with Degradability Kinetics Matching Healing Rates of Injured Bone. *Adv. Eng. Mater.* **2010**, *12* (11), B642−B648.

DOI: 10.1021/acsbiomaterials.7b00029
ACS Biomater. Sci. Eng. 2017, 3, 590−600

(48) Gaharwar, A. K.; Kishore, V.; Rivera, C.; Bullock, W.; Akkus, O.; Schmidt, G. Physically Crosslinked Nanocomposites from Silicate-Crosslinked PEO: Mechanical Properties and Osteogenic Differentiation of Human Mesenchymal Stem Cells. *Macromol. Biosci.* **2012**, *12*, 779−793.
(49) Gaharwar, A. K.; Schexnailder, P.; Kaul, V.; Akkus, O.; Zakharov, D.; Seifert, S.; Schmidt, G. Highly Extensible Bio-Nanocomposite Films with Direction-Dependent Properties. *Adv. Funct. Mater.* **2010**, *20*, 429−436.
(50) Schexnailder, P. J.; Gaharwar, A. K.; Bartlett, R. L., II; Seal, B. L.; Schmidt, G. Tuning Cell Adhesion by Incorporation of Charged Silicate Nanoparticles as Cross-Linkers to Polyethylene Oxide. *Macromol. Biosci.* **2010**, *10*, 1416−1423.
(51) Chen, H.; Yuan, L.; Song, W.; Wu, Z.; Li, D. Biocompatible Polymer Materials: Role of Protein−Surface Interactions. *Prog. Polym. Sci.* **2008**, *33*, 1059−1087.
(52) Gaharwar, A. K.; Schexnailder, P. J.; Kline, B. P.; Schmidt, G. Assessment of using Laponite cross-linked poly(ethylene oxide) for controlled cell adhesion and mineralization. *Acta Biomater.* **2011**, *7*, 568−577.
(53) Song, W.; Kawazoe, N.; Chen, G. Dependence of Spreading and Differentiation of Mesenchymal StemCells onMicropatterned Surface Area. *J. Nanomater.* **2011**, *2011*, 1.
(54) Kerativitayanan, P.; Carrow, J. K.; Gaharwar, A. K. Nanomaterials for Engineering Stem Cell Responses. *Adv. Healthcare Mater.* **2015**, *4* (11), 1600−1627.
(55) Zaky, S. H.; Lee, K.-W.; Gao, J.; Jensen, A.; Close, J.; Wang, Y.; Almarza, A. J.; Sfeir, C. Poly (glycerol sebacate) elastomer: a novel material for mechanically loaded bone regeneration. *Tissue Eng., Part A* **2013**, *20* (1−2), 45−53.
(56) Zhao, X.; Wu, Y.; Du, Y.; Chen, X.; Lei, B.; Xue, Y.; Ma, P. X. A highly bioactive and biodegradable poly (glycerol sebacate)−silica glass hybrid elastomer with tailored mechanical properties for bone tissue regeneration. *J. Mater. Chem. B* **2015**, *3* (16), 3222−3233.
(57) Yang, K.; Zhang, J.; Ma, X.; Ma, Y.; Kan, C.; Ma, H.; Li, Y.; Yuan, Y.; Liu, C. β-tricalcium phosphate/poly (glycerol sebacate) scaffolds with robust mechanical property for bone tissue engineering. *Mater. Sci. Eng., C* **2015**, *56*, 37−47.

DOI: 10.1021/acsbiomaterials.7b00029
ACS Biomater. Sci. Eng. 2017, 3, 590−600